Sea Ice Identification and Derivation of Its Velocity Field by X-Band Doppler Radar

YASUSHI FUJIYOSHI

Institute of Low Temperature Science, Hokkaido University, Sapporo, Japan

KOJI OSUMI*

Graduate School of Environmental Science, Hokkaido University, Sapporo, Japan

MASAYUKI OHI

J2 Co. Ltd., Minato, Japan

YOSHINORI YAMADA

Meteorological Research Institute, Japan Meteorological Agency, Ibaraki, Japan

(Manuscript received 26 July 2012, in final form 9 December 2012)

ABSTRACT

In this study a 3D scanning X-band Doppler radar (XDR) was deployed near the coast of the Sea of Okhotsk, Hokkaido, Japan, in November 2005 to simultaneously observe sea ice and snow clouds. Doppler radars are commonly used to detect wind fields within precipitating clouds. However, thus far, there have been no reports of observing sea ice with Doppler radar. Making use of the radar reflectivity, Doppler velocity, and spectrum width, sea ice floes were identified under various weather conditions. Also presented is a new method that combines Doppler radar data and sea ice velocity—extracted using the cross-correlation method—to derive a high-spatial-resolution horizontal distribution of the velocity of sea ice floes. These methods will contribute to short-term forecasting of sea ice conditions and navigation through ice-covered seas and the development and verification of high-resolution dynamic sea ice models.

1. Introduction

Many authors have reported on the shrinkage of the extent of Arctic sea ice in recent decades (e.g., Serreze et al. 2007) based on satellite imagery. Since marine transportation through the Arctic Ocean has been made possible now, the development of techniques to detect sea ice floes and forecast their movement with high temporal and spatial resolution is essential for transportation in ice-covered seas. Traditionally, ship- and land-based radars only make use of radar reflectivity to detect sea ice floes and forecast their movements over short periods of time (e.g., Tabata 1972). However, this technique does not work well under windy, snowy, and rainy conditions because of the masking effect of sea, snow, and rain echoes on sea ice echoes (see section 2 for details).

High-resolution representations of the temporal and spatial distribution of sea ice velocity fields are essential for short-term forecasting of sea ice conditions and navigation through ice-covered seas, and they are also indispensable for the development and verification of high-resolution dynamic sea ice models (Leppäranta 2005). Sea ice velocity can be extracted from sequential remote sensing (using both satellite- and ground-based radars as well as satellite-based visible/thermal IR) imagery using the cross-correlation method (e.g., Ishida 1974; Kimura and Wakatsuchi 2000; Inoue 2004; Kimura 2005; Mahoney et al. 2007). However, the extracted sea ice velocity has several uncertainties that cannot be

* Current affiliation: Geospatial Information Authority of Japan, Ibaraki, Japan.

Corresponding author address: Yasushi Fujiyoshi, Institute of Low Temperature Science, Hokkaido University, N19W8, Sapporo 0600819, Japan.
E-mail: fujiyo@lowtem.hokudai.ac.jp

DOI: 10.1175/JTECH-D-12-00155.1

corrected by the cross-correlation method itself. For example, when a completely circular ice disc rotates at a fixed point, this method cannot measure its rotation speed; when a target ice floe drastically changes its shape or disappears in a very short period of time because of melting and aggregation, its velocity cannot be extracted using this method. Therefore, the derived sea ice velocity should be verified by other methods. An automatic data buoy (e.g., the Argos system) deployed on sea ice can track its motion (Colony and Thorndike 1984). However, there are disadvantages to this method: the cost of drifters and the low temporal and spatial resolution. Acoustic Doppler current profilers can measure the speed of movement of sea ice (e.g., Fukamachi et al. 2011), but they cannot measure the spatial distribution of motion vectors.

We report on a technique for the detection of sea ice floes using Doppler radar data (radar reflectivity, radial velocity, and velocity spectrum width) obtained under various weather conditions. We also present a new method to derive a high spatial horizontal distribution of sea ice floe velocities.

2. Sea ice floe detection under various weather conditions

The north coast of Hokkaido, Japan, experiences seasonal sea ice. Usually, sea ice spreads southward along Sakhalin, reaches Hokkaido by mid-January, and retreats from Hokkaido in early April. The coastal C-band plan position indicator (PPI) radar system of the Sea Ice Research Laboratory of the Institute of Low Temperature Science (ILTS), Hokkaido University, Japan, had been continuously mapping the area of sea ice near the coast of the Sea of Okhotsk (Tabata 1972) since 1969 and terminated its 30 years of observation in 2004. Based on analysis of these data, Aota (1999) found a marked decreasing trend in sea ice extent in the Sea of Okhotsk.

We deployed a 3D scanning X-band Doppler radar (XDR) at Mt. Ooyama (44°20′33″N, 143°19′28″E; 313 m above sea level), Monbetsu City, Hokkaido, in November 2005 to simultaneously observe the developed sea ice and snow clouds over the Sea of Okhotsk (Fig. 1). Doppler radars are commonly used to detect wind fields within precipitating clouds. However, thus far, there have been no reports of using Doppler radar to observe sea ice. XDR can measure the three-dimensional backscattering intensity, Doppler velocity, and Doppler spectral width every 6 min. Operationally, we used four elevation angles (−0.5°, 0°, +0.5°, and 1.0°) to detect the horizontal distribution of sea ice and more than 13 elevation angles (0°–40°) to observe the three-dimensional

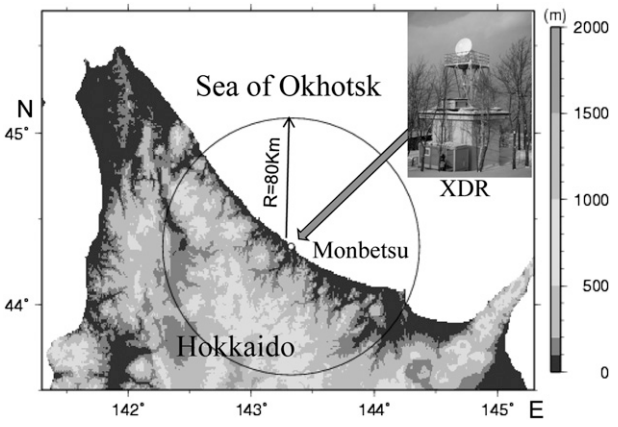

FIG. 1. Radar site (44°20′33″N, 143°19′28″E), radar coverage area, and outlook of Monbetsu XDR.

structure of precipitating clouds. The range and velocity resolutions were 100 m and 7 cm s^{-1}, respectively. The rotation speed of the antenna was 18° s^{-1} (3 rpm). The pulse width and pulse repetition frequency were 0.9 μs and 1000 Hz, respectively. The minimum detection range was 250 m. Although the maximum detection range of the XDR was 83.3 km, it could not detect sea ice farther than 60 km away because of the curvature of the earth. Figure 2 shows the *Aqua* Moderate Resolution Imaging Spectroradiometer (MODIS) imagery of sea ice at 1253 Japan standard time (JST) (UTC + 9 h) 23 January 2008, and the horizontal distribution of sea ice detected by XDR at 1243 JST. Similar to the former sea ice C-band radars, XDR can detect sea ice very well, at least within a range of 60 km under fine weather conditions.

Even if there are no snow clouds, sea ice floes are difficult to detect under windy conditions because both the echo intensity and the radial velocity of small-scale wind-roughened features on the sea surface (sea clutter) are almost the same as those of sea ice floes, as shown in Figs. 3a and 3b. The amount of sea spray is much smaller over the sea ice area, and ''spray'' over the sea might be one of the parameters contributing to the ''noise'' of the radar signals from the sea surface (Valenzuela and Lang 1970). Therefore, the Doppler spectrum width, which is a function of the spread of the radial velocity of scatterers, is quite useful for identifying areas of sea ice under windy conditions. Figure 3c shows the horizontal distribution of the Doppler spectrum width at 1901 JST 20 March 2012. Figure 4 shows the appearance frequency of the Doppler spectrum width (the area of range is 15–50 km and the azimuth is 300°–100° in Fig. 3c). The Doppler spectrum width of sea ice floes is lower than 0.3 m s^{-1} (Fig. 4), and that of sea clutter is greater than 0.4 m s^{-1}. On the basis of this information, we were

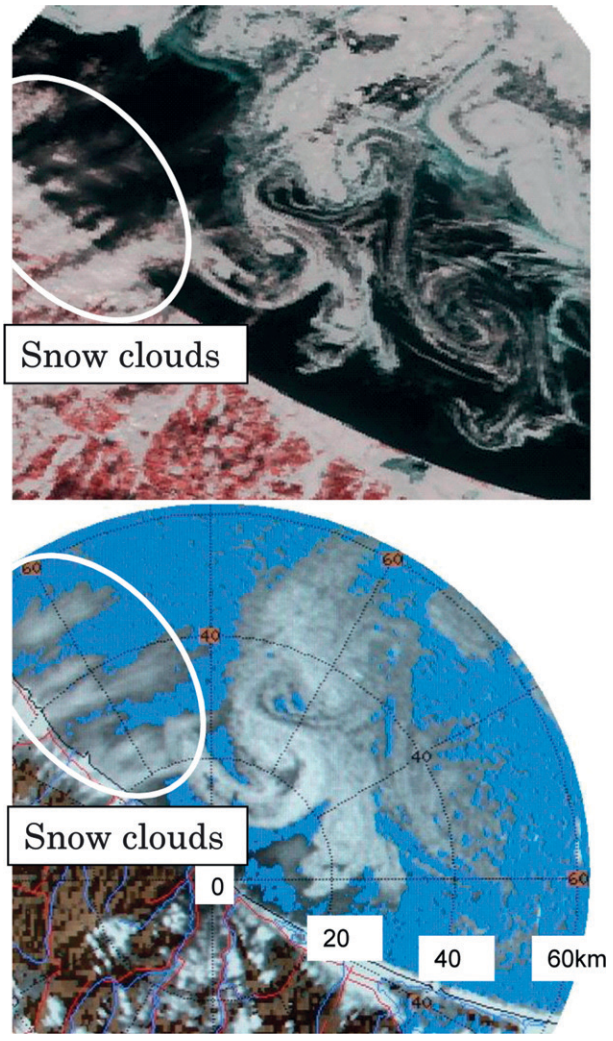

FIG. 2. Satellite (*Aqua* MODIS) imagery at 1253 JST (UTC+9 h) courtesy of Tokai University Space Information Center, Japan, and XDR PPI (elev = −0.5°) imagery at 1243 JST 23 Jan 2008. Note that the projection of the satellite image does not match the radar. Snow clouds seen in the western part of the top figure (within a white circle) were also clearly detected by the XDR.

able to identify areas of sea ice (Fig. 3c). However, the low signal intensity of the Doppler spectrum width lowers the maximum detection range (which is typically less than 50 km for our XDR).

Since the X-band radar is quite sensitive to snow particles, it is difficult to identify sea ice area during snowfall as exemplified in Fig. 5a; therefore, we developed several simple methods to address this issue. One method utilizes the difference in the moving velocity between sea ice and snow clouds. In general, sea ice floes move much more slowly than snow clouds. When we integrated the echo intensity with time at all sampling points, we observed that the intensity at points covered by sea ice was much higher than that at points covered only by snow clouds. Therefore, sea ice can be identified by displaying only those areas that have an integrated echo intensity greater than a given critical value. The Doppler velocity and the Doppler spectrum are also quite useful for identifying sea ice under snowy conditions as shown in Figs. 5b and 5c. The Doppler velocity and the Doppler spectrum of sea ice floes integrated with time are much smaller than those of snow clouds. Therefore, sea ice can be identified by displaying areas with a Doppler velocity and a Doppler spectrum below some critical values. We usually use 30 min for integration.

We can summarize the procedure to identify sea ice floes under various weather conditions as follows:

(i) Under clear and/or cloudy (no precipitation) skies
When surface winds are very weak and sea clutters do not appear, the echo intensity is enough to identify sea ice floes. When surface winds are strong and sea clutters appear, the Doppler spectrum is very useful to identify sea ice floes.

(ii) Under snowy conditions
Without regard to surface wind speed, the time integration method of the Doppler velocity and the Doppler spectrum is useful to identify sea ice floes. However, the best integration time and the threshold values should be empirically determined from place to place.

3. Methods to derive motion vectors of sea ice

a. Simple method to derive vorticity of sea ice floes

Before introducing a new method to derive high spatial velocity vector fields of sea ice, we present an example of the usefulness of Doppler radar to derive the mean vorticity of sea ice floes. Sea ice floes over the Sea of Okhotsk often exhibit fairly regular ocean wave motions in which some eddy streets or backward-breaking waves are present (Wakatsuchi and Ohshima 1990). The rotation speed of sea ice usually depends on its horizontal scale. The vorticity of 10-km-scale sea ice ranges from 10^{-7} to 10^{-5} s^{-1} (Leppäranta 2005). Individual motion vectors of sea ice floes are required to derive the vorticity. However, a vortex in solid rotation has a characteristic signature on a Doppler velocity display—that is, a pair of sharp velocity peaks. The distance between the maximum and minimum Doppler velocities D is defined as the "deduced core diameter" of a vortex. The deduced vertical vorticity ς is estimated from $2\Delta V/D$, where ΔV is the difference in Doppler velocity between the receding and approaching extrema in the vortex signature. Although this method is widely used to

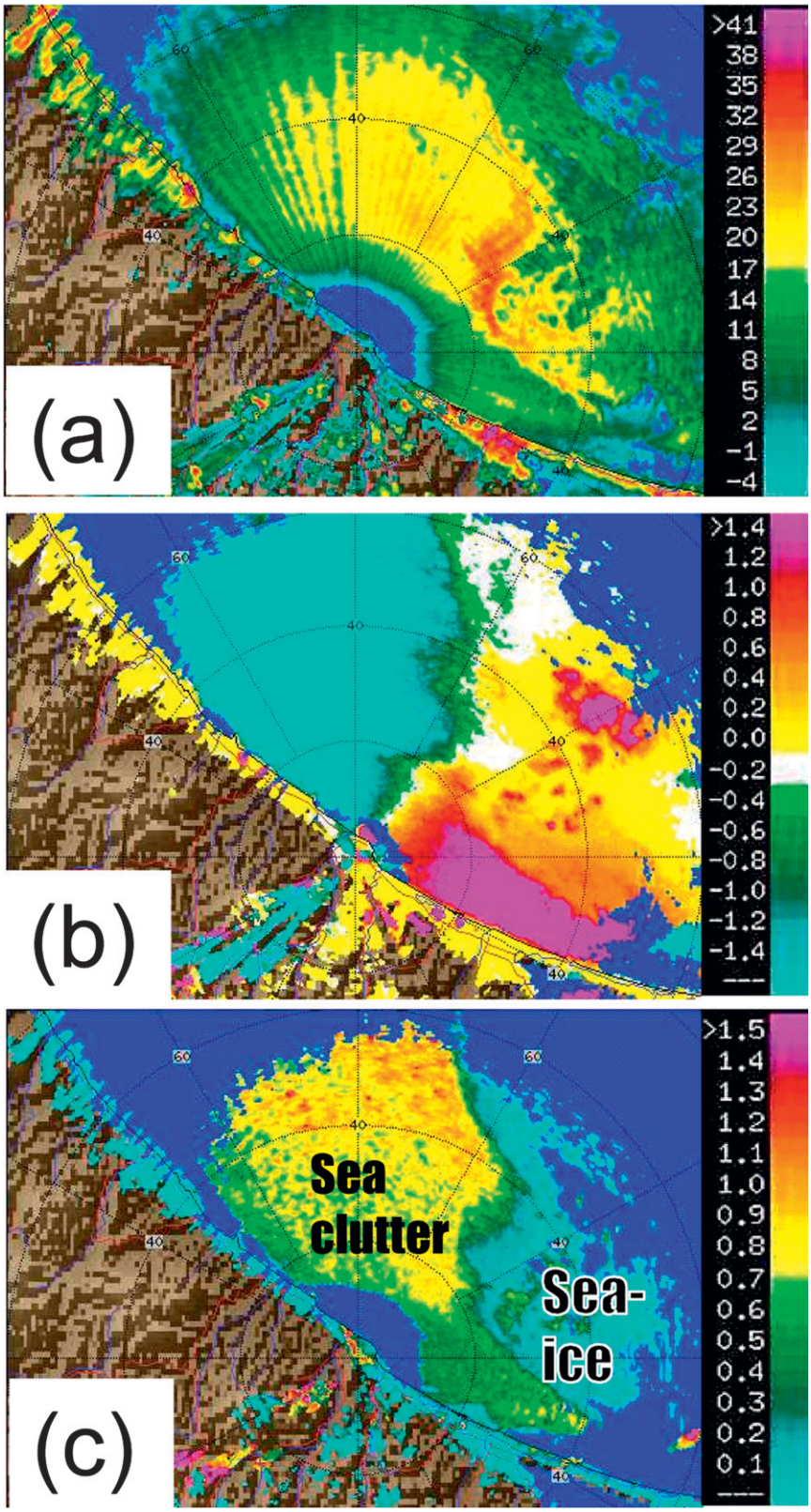

FIG. 3. PPI (elev = 1.1°) images of (a) radar echo intensity (dBZ), (b) Doppler velocity (m s^{-1}), and (c) Doppler spectrum width (m s^{-1}) at 1901 JST 20 Mar 2012.

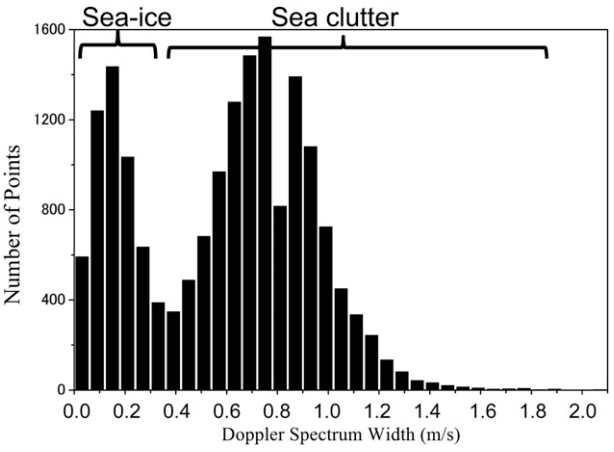

FIG. 4. Appearance frequency of Doppler spectrum width (area of range = 15–50 km and azimuth = 300°–100° in Fig. 3c).

detect vortex air motion in the atmosphere (e.g., Doviak and Zrnić 1993), it has not been applied to the detection of the rotation of sea ice.

Figure 6 shows the *Terra* MODIS imagery (Fig. 6a) taken at 1246 JST 28 March 2012, and the radial Doppler velocity imagery (Fig. 6b) of sea ice floes observed at 1231 JST. Figure 7 shows the azimuthal profile of the tangential Doppler velocity along line L1–L2 in Fig. 6b. The tangential component of the motion speed of eddy-A varied from -0.40 to $+0.47$ m s^{-1}. The core diameter and vertical vorticity of eddy-A were estimated to be about 9.4 km and 1.8×10^{-4} s^{-1}, respectively, and persisted at the same order of magnitude for at least 1 day (from 2000 JST March 27 to 2000 JST March 28). Overall, eddy-A rotated more or less as a rigid disc, although it was composed of many sea ice floes. However, in contrast to the Rankine combined vortex model, the tangential velocity of sea ice floes did not decrease sharply outside eddy-A; this may have been because of the high bulk viscosity of sea ice floes and the complicated motion of sea ice floes surrounding eddy-A (see arrows in Fig. 6b).

b. Comparison between extracted and observed Doppler velocity fields of sea ice

The complicated motion of sea ice floes at the sea ice edge off the Hokkaido coast was recognized through analysis of movie photography of ILTS C-band radars (e.g., Sonu and Aota 1985; Wakatsuchi and Ohshima 1990). Figure 8a shows PPI imagery of sea ice floes at 0504 JST 14 February 2010, when the sea ice floes exhibited an elongated spiral pattern. By applying the cross-correlation method to XDR data, we extracted sea ice motion data for the period between 0504 and 0534 JST (vectors in Fig. 8b). We compared calculated radial Doppler velocity fields of the extracted sea ice motion data as observable from the XDR site (Fig. 8b) with those obtained from the XDR observation (Fig. 8c). The two Doppler velocity fields were found to be quantitatively very similar. However, relatively large differences were found around the periphery of the sea ice area, where floes may have changed their shape because of melting and aggregation (dotted circles in Fig. 8b).

c. A new method to derive sea ice motion

A more reliable estimate of the sea ice velocity field was obtained by combining sea ice velocity components from the cross-correlation method with the corresponding Doppler velocity observations. This combined sea ice velocity can be derived from minimizing the function $J(u, v)$ on a plane (S), as follows:

$$J(u,v) = \int_S [A(u,v) + B(u,v,u_c,v_c) + C(u,v)]\, dS, \text{minimum}, \quad (1)$$

where u and v are the combined velocity components in the east–west and north–south directions, respectively; and u_c and v_c are the respective sea ice velocity components from the correlation method. In this equation, the first term indicates the interpolation of Doppler velocity data in polar coordinates (collected in PPI mode at an elevation angle of 0°) onto the grid points at which u_c and v_c were computed. Beam-by-beam processing was conducted as in Bousquet and Chong (1998) to avoid the so-called sampling problem. However, we utilized the practically useful interpolation form proposed by Yamada (2013).

The first tem of Eq. (1), A_{ij}, at grid point (i, j) can be written as follows:

$$A_{ij} = \mu_0 \frac{\sum_{q=1}^{n} \omega_q (\alpha_q u + \beta_q v - V_q)^2}{\sum_{q=1}^{n} \omega_q}, \quad (2)$$

where μ_0 is the prescribed weight, u and v are the combined sea ice velocity components at the grid point under consideration, α_q and β_q are the direction cosines of the qth beam of the radar, V_q is the Doppler velocity datum of the qth beam falling inside the influence circle, ω_q is the Cressman weight function (Cressman 1959) of V_q according to the distance from the center of the circle located at grid point (i, j), and n indicates the total number of velocity data points falling inside the influence

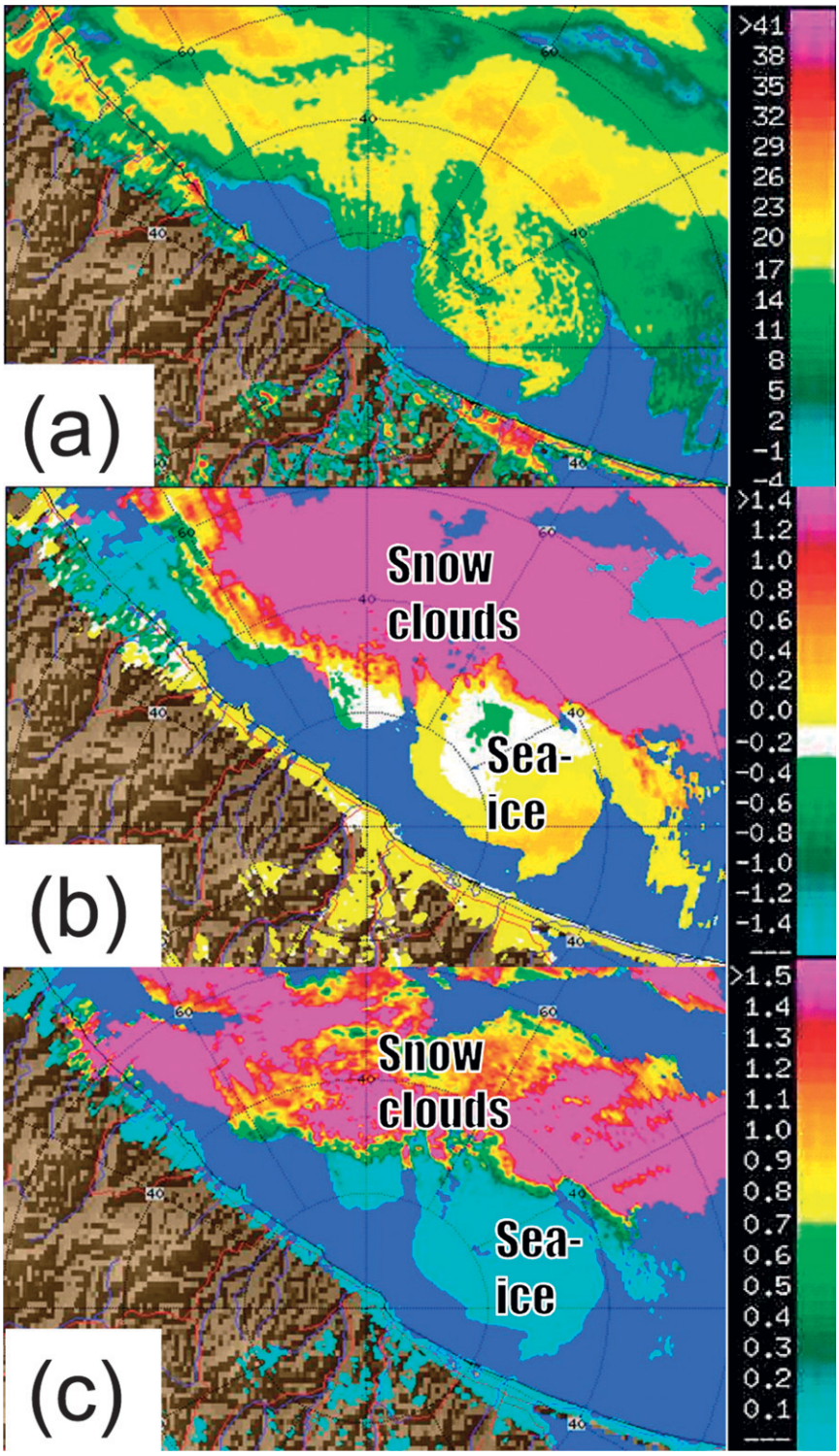

FIG. 5. PPI (elev = 1.1°) images of (a) radar echo intensity (dBZ) at 0001 JST 1 Mar 2012. (b) Doppler velocity (m s^{-1}) and (c) Doppler spectrum width (m s^{-1}) at 0007 JST.

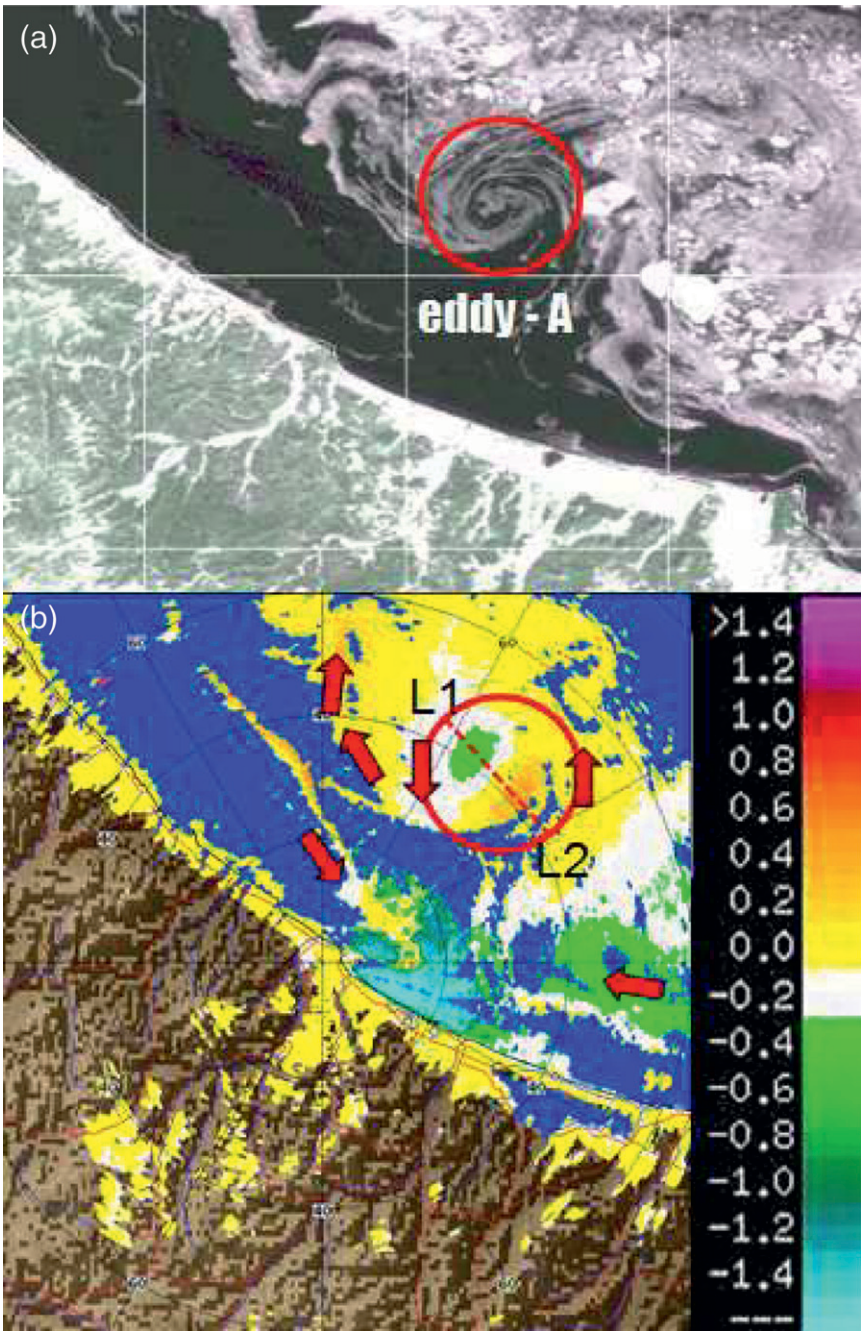

FIG. 6. (a) *Terra* MODIS imagery at 1246 JST 28 Mar 2012. (b) Radial Doppler velocity imagery of sea ice floes at 1231 JST. Arrows indicate the movement direction of sea ice floes.

circle. The vertical velocity component of sea ice floes was omitted. This term requires the combined velocity components in the radial direction to be close to the corresponding Doppler velocity.

The second term of Eq. (1), $B(u, v)$, indicates that the combined velocity components are close to the corresponding components from the correlation method in terms of least squares. This term may be formulated as follows:

$$B(u,v) = \mu_1[(u - u_c)^2 + (v - v_c)^2], \qquad (3)$$

where μ_1 is a predetermined weight. The third term of Eq. (1), $C(u, v)$, represents a filter term whose role is to

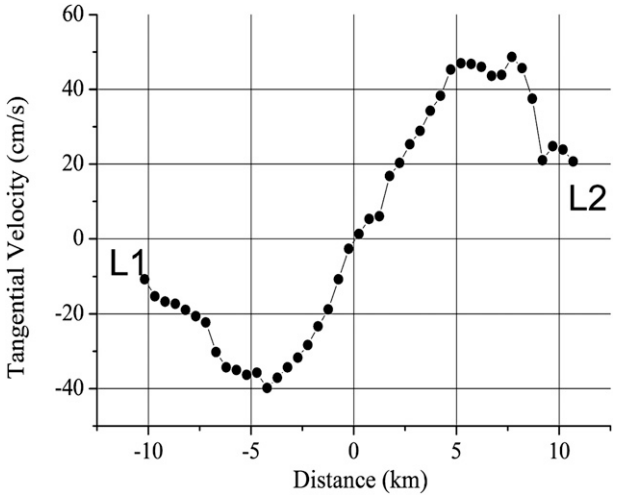

FIG. 7. Sea ice floes' vortex tangential velocity along the line L1–L2 in Fig. 6b.

eliminate smaller-scale variations as in Roux et al. (1984). More specifically, it may be written as follows:

$$C(u,v) = \mu_2 \left[\left(\frac{\partial^2 u}{\partial x^2} \right)^2 + 2 \left(\frac{\partial^2 u}{\partial x \partial y} \right)^2 + \left(\frac{\partial^2 u}{\partial y^2} \right)^2 + \left(\frac{\partial^2 v}{\partial x^2} \right)^2 + 2 \left(\frac{\partial^2 v}{\partial x \partial y} \right)^2 + \left(\frac{\partial^2 v}{\partial y^2} \right) \right]. \quad (4)$$

This is a spatially isotropic filter, and its filter characteristics are controlled by a weighting factor, which is related to the 3-dB cutoff wavelength λ_c, as follows:

$$\mu_2 = \left(\frac{\lambda_c}{2\pi} \right)^4. \quad (5)$$

The combined velocity components u and v are given by the solution of

$$\begin{cases} \dfrac{\partial J}{\partial u} = 0, \\ \dfrac{\partial J}{\partial v} = 0. \end{cases} \quad (6)$$

In practice, the combined velocity field was computed using five Doppler radar observations at 6-min intervals over a set interval in order to determine the sea ice velocity field from the correlation method. The horizontal grid resolution ($\Delta x = 0.25$ km) was the same as that for the correlation method. Each Doppler velocity data value was combined by first employing $\mu_0 = 1$, $\mu_1 = 5$, and $\lambda_c = 4\Delta x$. In this case, Doppler velocities at points with reflectivities ≥5 dBZ were

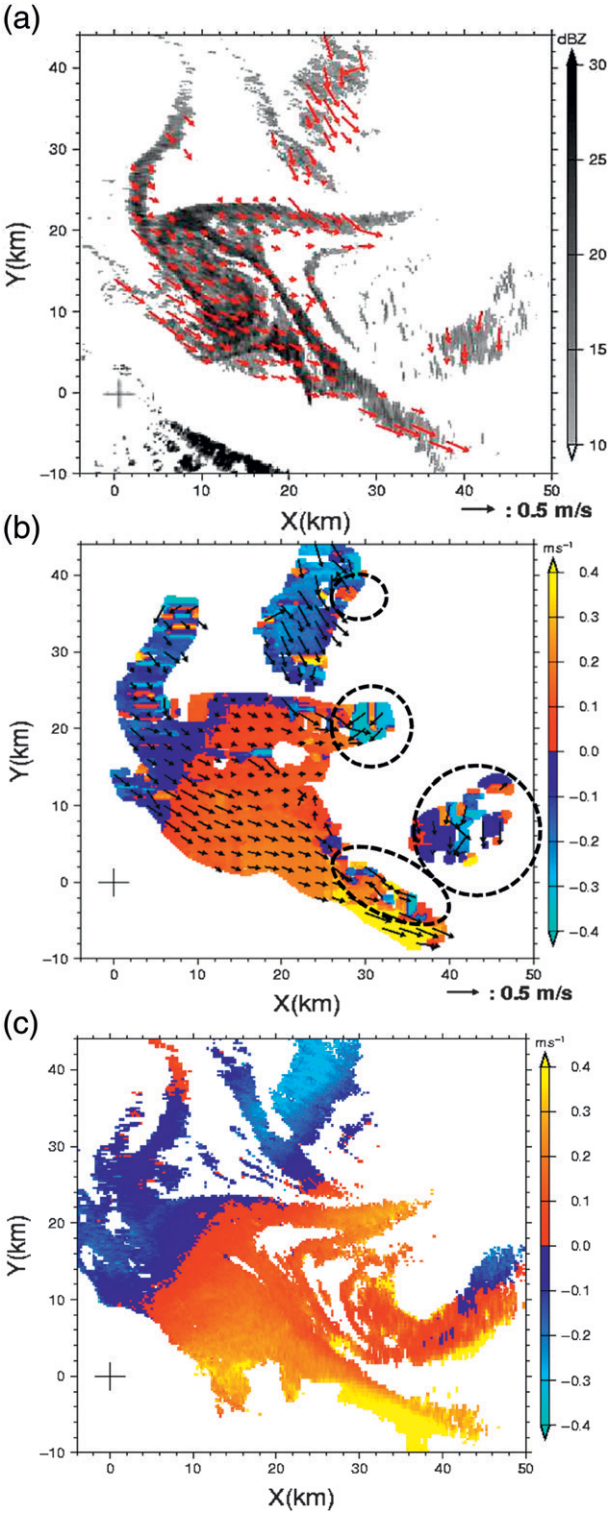

FIG. 8. (a) PPI imagery of sea ice floes at 0504 JST 14 Feb 2010, and estimated motion vectors of sea ice motion in the period between 0504 and 0534 JST. (b) Calculated radial Doppler velocity fields of the extracted sea ice motion as observed from the XDR site. (c) Observed radial Doppler velocity fields.

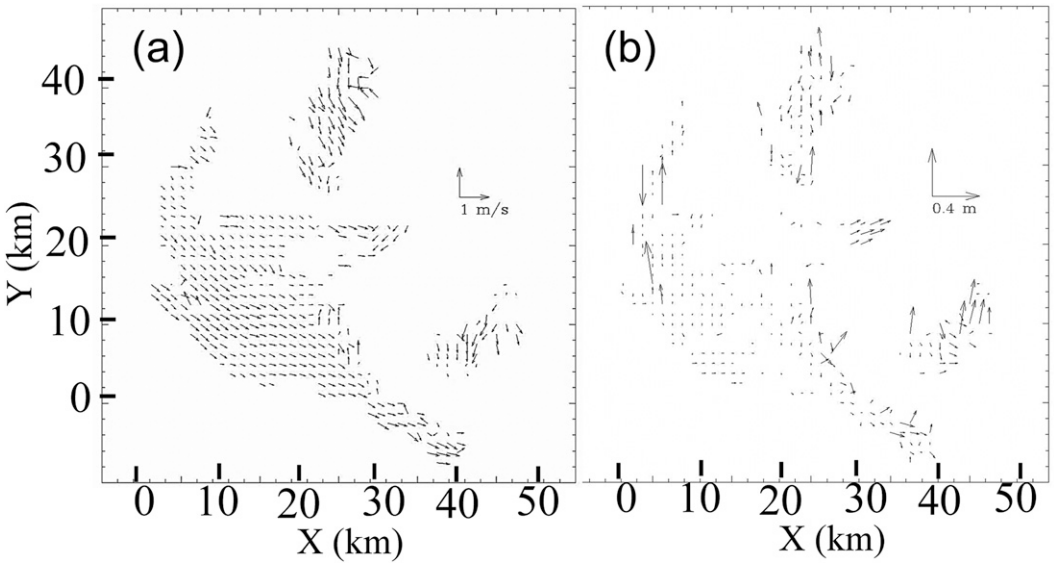

FIG. 9. (a) Combined velocity field of sea ice floes, and (b) the difference between motion vectors of sea ice floes derived from the combined and correlation methods. Vectors are plotted every five grids.

used. The final combined velocity components at each grid point were then obtained by taking the arithmetic mean of five points.

Figures 9a and 9b show the combined velocity field of sea ice floes and the difference between the motion vectors of sea ice floes derived from the combined and cross-correlation methods, respectively. Overall, the combined field did not significantly differ from that derived from the cross-correlation method. However, the velocity field (speed and/or direction) around the outer periphery of the area of sea ice coverage was modified. In this case, a combination of Doppler measurements and the correlation method may provide a better estimate of the sea ice velocity field.

4. Conclusions

We described several methods by which XDR can be used to detect sea ice floes, even under snowy and windy conditions. We showed that reliable estimates of the sea ice velocity field can be obtained by combining sea ice velocities extracted from the cross-correlation method with the corresponding Doppler velocity observations. Dual- or multi-Doppler radar systems can be used to visualize the horizontal distribution of sea ice motion vectors very easily. However, the area over which motion vectors can be derived becomes much smaller. Furthermore, deployment of many Doppler radars along the coast would be expensive. Thus, the methods presented here are recommended for future monitoring and warning systems for sea ice.

Although further study is required to confirm and determine some parameters, the methods presented here are useful for short-term forecasting of sea ice motion. In general, sea ice shows complicated motions, especially in marginal ice zones where mesoscale to small-scale eddies and whorls occur. Two important future tasks are assimilating XDR data into elastic–viscous–plastic sea ice models (e.g., Hunke and Dukowicz 1997; Rheem et al. 1997; Yamaguchi 2010) and measuring ice thickness. Our radars can scan in three dimensions to produce three-dimensional displays of snow clouds and sea ice (not shown). These images suggest that our radar system can be used to study height irregularities of the sea ice area (Fujiyoshi and Ohi 2009). By using an airborne high-resolution stereocamera and XDR, we intend to observe sea ice on February 2014 and will report the results in a subsequent paper.

Acknowledgments. This research was partially supported by the Ministry of Education, Culture, Sports, Science, and Technology Grant-in-Aid for Scientific Research (A) 21241045, 2009–11.

REFERENCES

Aota, M., 1999: Long-term tendencies of sea ice concentration and air temperature in the Okhotsk Sea coast of Hokkaido. Proceedings of the Second PICES Workshop on the Okhotsk Sea and Adjacent Areas, V. B. Lobanov, Y. Nagata, and S. C. Riser, Eds., North Pacific Marine Science Organization PICES Scientific Rep. 12, 1–2.

Bousquet, O., and M. Chong, 1998: A multiple-Doppler synthesis and continuity adjustment technique (MUSCAT) to recover

wind components from Doppler radar measurements. *J. Atmos. Oceanic Technol.,* **15,** 343–359.

Colony, R., and A. S. Thorndike, 1984: An estimate of the mean field of Arctic sea ice motion. *J. Geophys. Res.,* **89** (C6), 10 623–10 629.

Cressman, G. W., 1959: An operational objective analysis system. *Mon. Wea. Rev.,* **87,** 367–374.

Doviak, R. J., and D. S. Zrnić, 1993: *Doppler Radar and Weather Observations*. 2nd ed. Academic Press, 562 pp.

Fujiyoshi, Y., and M. Ohi, 2009: Doppler radar observation of sea ice, snow clouds and bird. *Proc. 24th Int. Symp. on Okhotsk Sea and Sea Ice,* Mombetsu, Japan, The Okhotsk Sea and Cold Ocean Research Association, 135–137.

Fukamachi, Y., K. I. Ohshima, Y. Mukai, G. Mizuta, and M. Wakatsuchi, 2011: Sea ice drift characteristics revealed by measurement of acoustic Doppler current profiler and ice-profiling sonar off Hokkaido in the Sea of Okhotsk. *Ann. Glaciol.,* **52,** 1–8.

Hunke, E. C., and J. K. Dukowicz, 1997: An elastic–viscous–plastic model for sea ice dynamics. *J. Phys. Oceanogr.,* **27,** 1849–1867.

Inoue, J., 2004: Effects of tidal current and wind on the coastal sea ice motion in the Sea of Okhotsk (in Japanese). *Sea Sky,* **79,** 57–64.

Ishida, K., 1974: Calculation of flow-vector of open pack-ice by 2-dimensional correlation method (in Japanese). *Low Temp. Sci.,* **32A,** 221–227.

Kimura, N., 2005: Sea ice motion derived from images by Aqua/AMSR-E. *Proc. 28th Symp. on Polar Meteorology and Glaciology,* Tokyo, Japan, National Institute of Polar Research, 53 pp.

——, and M. Wakatsuchi, 2000: Relationship between sea ice motion and geostrophic wind in the Northern Hemisphere. *Geophys. Res. Lett.,* **27,** 3735–3738.

Leppäranta, M., 2005: *The Drift of Sea Ice*. Springer, 266 pp.

Mahoney, A., H. Eicken, and L. Shapiro, 2007: How fast is landfast sea ice? A study of the attachment and detachment of near-shore ice at Barrow, Alaska. *Cold Reg. Sci. Technol.,* **47,** 233–255.

Rheem, C. K., H. Yamaguchi, and H. Kato, 1997: Distributed mass/discrete floe model for pack ice rheology computation. *J. Mar. Sci. Technol.,* **2,** 101–121.

Roux, F., J. Testud, M. Payen, and B. Pinty, 1984: West African squall-line thermodynamic structure retrieved from dual-Doppler radar observations. *J. Atmos. Sci.,* **41,** 3104–3121.

Serreze, M. C., M. M. Holland, and J. Stroeve, 2007: Perspectives on the Arctic's shrinking sea-ice cover. *Science,* **315,** 1533–1536.

Sonu, C. J., and M. Aota, 1985: Characteristic ice floe movements as revealed by shore-based radars. *Proc. 17th Offshore Technology Conf.,* Houston, TX, The Marine Technology Society, 353–355.

Tabata, T., 1972: Radar network for drift ice observations in Hokkaido. *Sea Ice: Proceedings of an International Conference,* T. Karlsson, Ed., National Research Council, 67–71.

Valenzuela, G. R., and M. B. Lang, 1970: Study of Doppler spectra of radar sea echo. *J. Geophys. Res.,* **75** (3), 551–563.

Wakatsuchi, M., and K. I. Ohshima, 1990: Observations of ice-ocean eddy streets in the Sea of Okhotsk off the Hokkaido coast using radar images. *J. Phys. Oceanogr.,* **20,** 585–594.

Yamada, Y., 2013: Characteristics of MUSCAT-derived wind fields. *J. Meteor. Soc. Japan,* in press.

Yamaguchi, H., 2010: Numerical prediction of sea ice change in the Sea of Okhotsk. *Proc. 25th Int. Symp. on Okhotsk Sea and Sea Ice,* Mombetsu, Japan, The Okhotsk Sea and Cold Ocean Research Association, 6–11.